

# Computationally Efficient Strategy for Modeling the Effect of Ion Current Modifiers

David G. Rand, Qinlian Zhou, Gregory T. Buzzard, and Jeffrey J. Fox\*

**Abstract**—Electrophysiological studies often seek to relate changes in ion current properties caused by a chemical modifier to changes in cellular properties. Therefore, quantifying concentration-dependent effects of modifiers on ion currents is a topic of importance. In this paper, we sought a mathematical method for using ion current data to predict the effect of several theoretical ion current modifiers on cellular and tissue properties that is computationally efficient without compromising predictive power. We focused on the  $K^+$  current  $I_{K,r}$  as an example case due to its link to long QT syndrome and arrhythmias, but these methods should be generally applicable to other electrophysiological studies. We compared predictions using a Markov model with mass action binding of the modifiers to specific conformational states of the channel to predictions generated by two simplified models. We investigated scaling  $I_{K,r}$  conductance, and found that although this method produced predictions that agreed qualitatively with the more complicated model, it did not generate quantitatively consistent predictions for all modifiers tested. Our simulations showed that a more computationally efficient Hodgkin–Huxley model that incorporates the effect of modifiers through functional changes in the current produced quantitatively consistent predictions of concentration-dependent changes in cell and tissue properties for all modifiers tested.

**Index Terms**—Computer simulation, electropharmacology, electrophysiology, mathematical modeling.

## I. INTRODUCTION

**M**ATHEMATICAL modeling and computational simulations have a long history of use in electrophysiology, dating back to the seminal work of Hodgkin and Huxley [1]. One of the primary questions that mathematical tools have been used to address is how ion currents that flow through a variety of types of ion channels control the membrane potential to generate the rich dynamics that are observed in cells [2]. For example, the electrical behaviors exhibited by cells can include oscillations in cardiac pacemaker cells [3] and neurons [4], bursting in pancreatic B-cells [5], and excitability in cardiac ventricular cells [6] and Purkinje fibers [7]. The rapid increase and subsequent return to rest of the membrane potential in excitable and oscillatory cells is often called an action potential (AP).

Manuscript received September 8, 2006; revised March 8, 2007. These studies were supported in part by the National Institutes of Health (NIH) under Grant R43 HL077938, Grant R01 HL075515, Grant R43 HL081687, Grant R43 HL079709, and by the National Science Foundation (NSF) under Grant DMS-0408293. Asterisk indicates corresponding author.

\*J. Fox is with Gene Network Sciences, Ithaca, NY 14850 USA (e-mail: jeff@gnsbiotech.com).

D. Rand is with the Program for Evolutionary Dynamics, Harvard University, Cambridge, MA 02138-3758 USA (e-mail: drand@fas.harvard.edu).

G. Buzzard is with the Department of Mathematics, Purdue University, West Lafayette, IN 47907 USA (e-mail: buzzard@math.purdue.edu).

Q. Zhou is with Gene Network Sciences, Ithaca, NY 14850 USA.

Color versions of one or more of the figures in this paper are available online at <http://ieeexplore.ieee.org>.

Digital Object Identifier 10.1109/TBME.2007.896594

Mathematical models have been used to explain cellular behaviors such as the AP in terms of the dynamics of the important ion currents in each cell type [8]. An important feature of many of these models is that the conductance of a particular ion channel can be time and voltage dependent [2]. The change in conductance of an ion channel is often modeled as a set of nonlinear differential equations describing the opening and closing of one or more independent gates, following the formalism introduced by Hodgkin and Huxley [1]. An alternative description called a Markov gating model describes voltage-dependent transitions between discrete states that correspond to different physical conformations of the channel proteins [9].

Often electrophysiologists are interested in studying the response of cellular electrical activity to a perturbation in the cellular environment. For example, a researcher might wish to observe the response of a single (or multiple) ion current(s) to a chemical that modifies the properties of that current, and then to relate the changes in the current to changes in cellular behavior. Some particularly important electrophysiological modifiers include natural toxins [10], drugs designed to treat central nervous system disorders [11], cellular kinases that phosphorylate channels [12], and second messenger molecules such as  $Ca^{2+}$  ions [13] and cAMP [14] that are used to relay important cellular signals. In addition, some compounds that are designed to treat disorders from a wide range of therapeutic areas have been found to interrupt the normal activity of cardiac ion currents in potentially dangerous ways [15]. One ion current in particular, the delayed rectifier potassium current  $I_{K,r}$ , that results from expression of the HERG gene, appears to be an unwanted target of many compounds that have been shown to induce abnormal cardiac rhythms [16], including a dangerous and potentially fatal arrhythmia called Torsades de Pointes [15]. Quantifying the effects of ion current modifiers on the electrical properties of individual ion currents and on cellular properties could help electrophysiologists understand why certain compounds might induce harmful, or helpful, changes in ion currents and cellular behaviors.

Several experimental methods exist for measuring the effect of a modifier on an ion channel, including voltage clamp assays, binding assays, and fluorescence assays [17]. Voltage clamp assays involve measurements of current generated in response to voltage command protocols in isolated cells. Change in normalized peak current in response to voltage clamp stimulation using voltage step command protocols [18]–[20] or AP command protocols [20]–[23] is often used to measure the effect of the modifier on the current.

Ideally, the results of an experimental characterization of a modifier's effect on an ion current could be used to predict likely changes in cellular and tissue electrophysiological properties. To predict changes in cellular or tissue properties based on ion

current data, it is necessary to incorporate concentration-dependent effects of the modifier into an accurate model of the ion current. Furthermore, it is desirable to minimize the complexity of the model so as to reduce the computational resources necessary to fit the model to data.

A common method for modeling the effect of a modifier on an ion current is to fit the normalized peak current concentration-response data to a standard sigmoid curve. In this case, the half-maximal response parameter, the  $EC_{50}$  (or  $IC_{50}$  for ion current inhibitors) can be used to quantify the modifier's effect on the ion current. While this method has the advantage of simplicity, it has been shown that the measured value of this parameter can depend on the experiment that is used to measure the effect of the modifier on the current. For example, some compounds that inhibit  $I_{K,r}$  have been shown to have different  $IC_{50}$  values when the  $I_{K,r}$  current is measured under different stimulus patterns [24].

Another more complicated method used to model the effect of a modifier involves constructing Markov state transition models of the binding of the modifying compound to the ion channel [25]. Models constructed according to this formalism attempt to reflect the physical interaction of the ion channel and the modifier under study. This method often uses prior knowledge of the binding properties of the modifier to reduce the number of unknown parameters. Alternatively, modeling the effect a novel modifier with unknown binding properties requires the estimation of a large number (which can increase quickly depending on the complexity of the modifier/ion channel interactions) of parameters. Consequently, a method that is less computationally intensive but has equal predictive power would be highly advantageous.

In this paper, we sought an approach for mathematically modeling the effect of a modifier on an ion current that produces quantitative predictive agreement with a Markov model without requiring either prior knowledge of the physical properties of the modifier or extensive computation. Such a model could be used to predict changes in cellular and tissue properties as a function of modifier concentration for novel compounds based on experimentally collected ion current concentration-response data. To evaluate models of the effect of the modifier in this paper, we modeled binding of compounds that block  $I_{K,r}$ . This ion current was chosen because it has been extensively studied due to its association with the lengthening of the QT interval of the electrocardiogram (ECG) and life-threatening cardiac arrhythmias such as Torsades de Pointes (TdP) [15]. Although the exact mechanism by which an  $I_{K,r}$  blocker may induce TdP remains unknown, the arrhythmogenic properties of such modifiers have been hypothesized to involve the amplification of intrinsic electrical heterogeneity in the ventricular tissue, caused by preferential prolongation of the midmyocardial (M) cell action potential duration (APD) relative to epicardial and endocardial cell APD [26]. Thus,  $I_{K,r}$  represents an ideal current for use in developing a method for incorporating concentration-dependent effects of an ion current modifier. However, the method developed in this paper is general and does not depend on the details of this particular current.

Using a Markov model with direct binding of the modifier, we created three theoretical modifiers and generated synthetic ion current data and APD concentration-response predictions

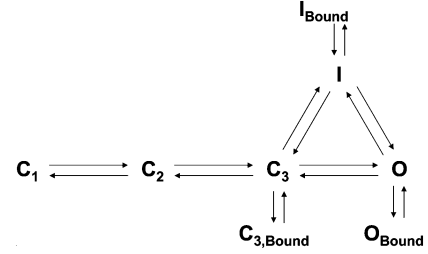


Fig. 1. State diagram of the  $I_{K,r}$  Markov model with modifier binding.  $C_1$ ,  $C_2$ , and  $C_3$  are closed states.  $O$  is the open state, and  $I$  is the inactive state. Each  $Y_{\text{bound}}$  state is a modifier-channel complex with the channel in state  $Y$ . Transitions from state to state are functions of voltage of the form  $A * \exp(B * V)$ , and modifier binding and unbinding rates are voltage independent functions of modifier concentration and state occupancy.  $I_{K,r}$  is a function of the population of state  $O$ .

for each. We then used these data to evaluate two alternate modeling methods for quantifying modifier-ion channel interactions, the commonly used method of scaling channel conductance as a function of concentration [19], [27] in a Markov model, and a novel method involving a Hodgkin–Huxley (HH) formulation. Previous work has related Markov and HH models by incorporating knowledge of a modifier's binding properties [28], but the method described here requires no such prior knowledge.

## II. METHODS

To study modifier-ion current interactions, we modeled the canine rapid inward delayed rectifier  $K^+$  current  $I_{K,r}$ , and its interaction with three theoretical modifiers, using three different mathematical formulations. First, we used a deterministic Markov model with mass action binding kinetics (Markov<sub>MB</sub>) to simulate the effect of modifiers that bind to particular states of the channel. Next, we used the same Markov control model of  $I_{K,r}$  and replaced mass action kinetics with scaling of channel conductance to model the effect of the modifier (Markov<sub>GKr</sub>). Last, we studied a method for using a Hodgkin–Huxley (HH) model with modifier dependence (HH<sub>Mod</sub>) as a framework for determining the functional consequences of the modifier-ion current interaction, such as changes in conductance, or activation and inactivation kinetics.

1) *Markov<sub>MB</sub> Model Topology*: The Markov model we studied follows the five state formulation given in [9] with three closed states ( $C_1$ ,  $C_2$ , and  $C_3$ ), one open state ( $O$ ), and one inactive state ( $I$ ). We examined the effect of three theoretical modifiers that preferentially bind a single conformational state of the  $I_{K,r}$  channel (see Fig. 1; modifiers binding states  $C_1$  and  $C_2$  produced similar results to the modifier binding state  $C_3$  and are, therefore, not discussed in the text). Mass-action kinetics was used to model binding and unbinding of a modifier to a given state of the Markov model, with each modifier assigned a binding rate  $k_{\text{on}}$  and an unbinding rate  $k_{\text{off}}$  (see Section II-A2). Although this model is a simplification of the physiological reality, it still allows for interesting and nonintuitive dynamics.

This formulation assumes that when a modifier binds a given conformational state, the channel cannot transition to a different conformational state until the modifier unbinds. That is, there are no transitions between bound states of the model (i.e.,

TABLE I  
 TRANSITION RATES FOR MARKOV MODEL OF  $I_{K,r}$ 

$C_1 \rightarrow C_2$	$\alpha_0 = 0.00414573 \times \exp(0.09856 \times V)$
$C_2 \rightarrow C_1$	$\beta_0 = 0.00291266 \times \exp(-0.0315044 \times V)$
$C_3 \rightarrow O$	$\alpha_1 = 0.000586909 \times \exp(0.0170419 \times V)$
$O \rightarrow C_3$	$\beta_1 = 0.000232786 \times \exp(-0.0567021 \times V)$
$O \rightarrow I$	$\alpha_i = 0.927666 \times \exp(0.0186985 \times V)$
$I \rightarrow O$	$\beta_i = 0.0138023 \times \exp(-0.0252146 \times V)$
$C_3 \rightarrow I$	$\alpha_{i3} = 0.00707894 \times \exp(3.49E-08 \times V)$
$I \rightarrow C_3$	$\psi = (\beta_1 \times \beta_i \times \alpha_{i3}) / (\alpha_1 \times \alpha_i)$
$C_2 \rightarrow C_3$	$K_f = 0.0441566$
$C_3 \rightarrow C_2$	$K_b = 0.272749$

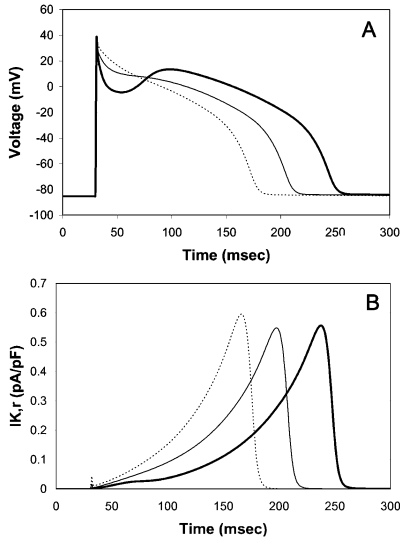


Fig. 2. (A) AP clamp command APs at (thick line) 1000 ms, (thin line) 500 ms, and (dotted line) 300 ms. (B) Control Markov  $I_{K,r}$  during AP clamp stimulation at (thick line) 1000 ms, (thin line) 500 ms, and (dotted line) 300 ms.

$I_{\text{Bound}} \rightarrow O_{\text{Bound}}$ ), only between bound and unbound states (i.e.,  $I_{\text{Bound}} \rightarrow I \rightarrow O \rightarrow O_{\text{Bound}}$ ). This approximation is valid for preferential binding of a single state as long as  $k_{\text{on}}$  (preferred state)  $\gg k_{\text{on}}$  (other states), and  $k_{\text{off}}$  (preferred state)  $\gg k_{\text{off}}$  (other states). Additionally, this model assumes that no current flows through the open state O when bound by Modifier<sub>O</sub>.

2) *Choice of Parameters:* To facilitate the study of the  $I_{K,r}$  Markov model in computer simulations of canine ventricular APs, transition rate parameters in the Markov model were chosen to qualitatively reproduce canine  $I_{K,r}$  recordings from previous experiments [29]. Transition rates for the control model are shown in Table I. AP clamp command protocol morphologies are shown in Fig. 2(a), and representative control  $I_{K,r}$  traces in Fig. 2(b).

The  $k_{\text{on}}$  and  $k_{\text{off}}$  rates for each modifier were chosen such that when stimulated with the voltage step protocol described in [9] ( $V = -80$  mV for 3 s,  $V = 10$  mV for 3.5 s,  $V = -50$  mV for 4 s), the IC<sub>50</sub> (concentration at which peak  $I_{K,r}$  is reduced by 50%) of the normalized peak  $I_{K,r}$  concentration-response curve for each modifier was 100 nM. For each modifier, a sequence of ten increasing concentrations was chosen to produce  $I_{K,r}$  block

 TABLE II  
 MODIFIER PARAMETERS FOR Markov<sub>MB</sub> MODEL

	Modifier <sub>C3</sub>	Modifier <sub>O</sub>	Modifier <sub>I</sub>
$K_{\text{on}}$	0.0360257	0.00013021	5.70106
$K_{\text{off}}$	0.1	0.1	0.1
Conc 1 – 0% $I_{K,r}$ block	0	0	0
Conc 2 – 10% $I_{K,r}$ block	19.3	11.0	11.0
Conc 3 – 20% $I_{K,r}$ block	34.2	24.9	23.8
Conc 4 – 30% $I_{K,r}$ block	51.0	42.7	41.7
Conc 5 – 40% $I_{K,r}$ block	72.0	66.5	65.9
Conc 6 – 50% $I_{K,r}$ block	100	100	100
Conc 7 – 60% $I_{K,r}$ block	141.2	150.3	151.4
Conc 8 – 70% $I_{K,r}$ block	208.8	234.5	237.6
Conc 9 – 80% $I_{K,r}$ block	342.7	403.3	410.5
Conc 10 – 90% $I_{K,r}$ block	742.5	912.6	931.9

Binding rate in nL·N·molecules<sup>-1</sup>·ms<sup>-1</sup>, unbinding rate in nL·N·ms<sup>-1</sup>, and concentrations in nM for Modifier<sub>C3</sub>, Modifier<sub>O</sub>, and Modifier<sub>I</sub>.

in increasing increments of 10%. See Table II for  $k_{\text{on}}$ ,  $k_{\text{off}}$ , and concentration values.

3) *Generation of Synthetic Data:* In this paper, we aimed to reproduce modifier-dependent changes in  $I_{K,r}$  during APs at various pacing rates. Therefore, we measured the *in silico* concentration-response of  $I_{K,r}$  when stimulated with an AP clamp protocol. To simulate an AP clamp protocol, steady-state APs from the Hund–Rudy AP model [30] at cycle lengths of 1000, 500, and 300 ms were applied to the model as command potentials (see [30, Appendix A, Sec. A.1.1] for command AP morphologies). Each AP was applied ten times to allow the modifier- $I_{K,r}$  model to reach steady state, and the  $I_{K,r}$  trace in response to the final AP at each cycle length was examined.

#### A. Concentration-Dependent Scaling of Markov Model Conductance (Markov<sub>GKr</sub>)

In addition to the Markov model with mass action binding presented in Section II-A1, this paper investigated an alternate method of modeling modifier interaction in a Markov model which involved scaling  $I_{K,r}$  conductance ( $GKr$ ) as a function of concentration. The same control Markov model of  $I_{K,r}$  described in Section II-A1 was used and  $GKr$  was varied with modifier concentration using the sigmoidal function given in (1)

$$Q(\text{conc}) = \frac{Q_0}{1 + \left(\frac{\text{conc}}{D_{Q,1/2}}\right)^{h_Q}} + \frac{Q_{\text{Inf}}}{1 + \left(\frac{D_{Q,1/2}}{\text{conc}}\right)^{h_Q}} \quad (1)$$

where  $Q$  is any given concentration-dependent quantity,  $\text{conc}$  is the concentration of the modifier in nanometers,  $Q_0$  is the value of  $Q$  when concentration = 0,  $Q_{\text{Inf}}$  is the value of  $Q$  as concentration approaches infinity,  $D_{Q,1/2}$  is the value of concentration at which the value of  $Q = (Q_0 + Q_{\text{Inf}})/2$ , and  $h_Q$  is the Hill Coefficient, determining the slope of the concentration-response for quantity  $Q$ . The four parameters  $Q_0$ ,  $Q_{\text{Inf}}$ ,  $D_{Q,1/2}$ , and  $h_Q$  for a given quantity  $Q$  are collectively referred to as the modifier-effect parameters for that quantity.

The modifier-effect parameters for  $GKr$  in the Markov<sub>GKr</sub> model were then fit to synthetic concentration-response AP clamp data generated by the Markov<sub>MB</sub> model at the ten modifier concentrations described in Section II-A3 using the Levenberg–Marquardt local optimization algorithm [31].

### B. Hodgkin–Huxley Model With Modifier Effect (HH<sub>Mod</sub>)

We utilized an HH model of  $I_{K,r}$  that follows the  $I_{K,r}$  formulation given in [29]. This model includes time dependence in both the activation gate ( $X$ ) and the inactivation gate ( $Y$ ). The HH model parameters were fit to control AP clamp data generated using the Markov model from Section II-A. The fit was performed using the Levenberg–Marquardt local optimization algorithm [31]. The formulations and parameters for our modified  $I_{K,r}$  model are as follows:

$$I_{K,r} = GK_r \times X \times Y \times (V - Ek) \quad (2)$$

$$\frac{dX}{dt} = \frac{X^\infty - X}{S_X \times \tau_x} \quad (3)$$

$$\frac{dY}{dt} = \frac{Y^\infty - Y}{S_Y \times \tau_y} \quad (4)$$

$$X^\infty = \frac{1}{1 + e^{-(V-R_X)/2.2}} \quad (5)$$

$$\tau_x = 10.1 + \frac{1}{e^{0.103(V-64.6)} + e^{-0.100(V+88.6)}} \quad (6)$$

$$Y^\infty = \frac{1}{1 + e^{(V-R_Y)/14.8}} \quad (7)$$

$$\tau_y = 0.51 + \frac{1}{e^{1.01(V+31.7)} + e^{-1.00(V+74.3)}} \quad (8)$$

where  $X$  and  $Y$  are the time- and voltage-dependent open probabilities of activation and inactivation gates,  $GK_r = 0.0502$  mS/uF is the conductance of  $I_{K,r}$ ,  $V$  is the membrane potential,  $Ek = -85.6$  mV is the reversal potential of the  $I_{K,r}$  channel,  $X^\infty$  and  $Y^\infty$  are the steady-state voltage-dependent open probabilities of the activation and inactivation gates  $\tau_x$  and  $\tau_y$  are the voltage-dependent activation and inactivation time constants  $R_X$  and  $R_Y$  are the crossover voltages of the steady values for the  $X$  and  $Y$  gates, and  $S_X$  and  $S_Y$  are scaling factors for the time constants of the  $X$  and  $Y$  gates. In the control model,  $R_X = -68.6$  mV,  $R_Y = -34.1$  mV,  $S_X = 1$ , and  $S_Y = 1$ .  $I_{K,r}$  traces generated by the HH model and “target” synthetic data generated by the control Markov simulation in response to an AP clamp at CL = 1000 and 300 ms are shown in Fig. 3.

To incorporate the effect of the modifier into the HH model, two alternate strategies were used. First, the effect of the modifier was modeled by allowing channel conductance  $GK_r$  to vary as a function of concentration according to (1), as described in Section II-B. If this method was not able to satisfactorily reproduce the  $I_{K,r}$  concentration-response target data, several additional model parameters which describe the functional characteristics of the  $I_{K,r}$  channel were allowed to vary as a function of modifier concentration: the crossover voltages of the steady values for the  $X$  and  $Y$  gates ( $R_X$  and  $R_Y$ ) and scaling factors for the time constants of the  $X$  and  $Y$  gates ( $S_X$  and  $S_Y$ ). We refer to these four parameters together with  $GK_r$  as the HH<sub>Mod</sub> quantities. Each of these quantities was then varied as a function of modifier concentration according to the sigmoidal formulation in (1).

This HH<sub>Mod</sub> model was then fit to synthetic concentration-response AP clamp data generated by the Markov<sub>MB</sub> model at the ten modifier concentrations described in Section II-A3. To determine the values of the modifier-effect parameters for each HH<sub>Mod</sub> quantity, a three step process was used. First,

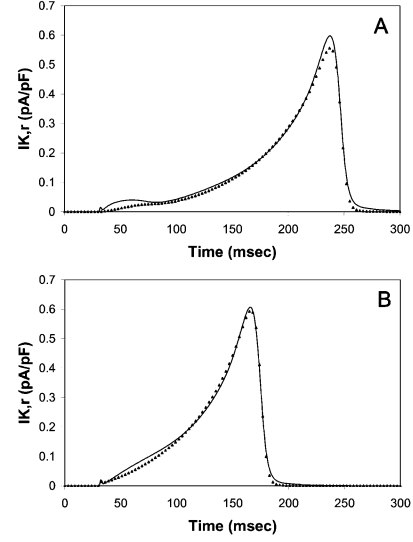


Fig. 3.  $I_{K,r}$  traces generated by (lines) HH control model and (triangles) Markov control model in response to an AP clamp. (A) CL = 1000 ms. (B) CL = 300 ms.

TABLE III  
MODIFIER-EFFECT PARAMETERS FOR HH<sub>Mod</sub> MODEL

	$Q_0$	$Q_{inf}$	$D_{1/2,Q}$	$h_Q$
<b>Modifier<sub>I</sub></b>				
GK <sub>r</sub>	0.0502	5.49385e-010	100	0.998918
<b>Modifier<sub>C3</sub></b>				
GK <sub>r</sub>	0.0502	0.000982728	12.8282	1.34577
<b>Modifier<sub>O</sub></b>				
GK <sub>r</sub>	0.09369	0.05351	364.652	0.526132
$S_X$	2.22409	19.1377	803.841	1.1119
$S_Y$	0.609499	196.466	2033.18	1.37646
$R_X$	-72.3022	-37.3184	171.548	0.395003
$R_Y$	-33.9829	48.0234	1957.13	0.655667

the HH<sub>Mod</sub> quantities themselves were optimized at each concentration, independent of model behavior at any other concentration. The fitted values of a given HH<sub>Mod</sub> quantity  $Q$  at each modifier concentration then form a concentration-response curve for  $Q$ . Second, this concentration-response curve for each HH<sub>Mod</sub> quantity  $Q$  was fit using (1) to determine initial values of the modifier-effect parameters  $Q_0$ ,  $Q_{inf}$ ,  $D_{Q,1/2}$ , and  $h_Q$ . Third, the modifier-effect parameters for all of the HH<sub>Mod</sub> quantities were optimized at the same time to data from all ten concentrations simultaneously. All optimizations were done using the Levenberg–Marquardt optimization algorithm with least squares cost function. The modifier effect parameter values which quantitatively reproduced the Modifier<sub>C3</sub>, Modifier<sub>I</sub>, and Modifier<sub>O</sub> concentration-response of AP clamp  $I_{K,r}$  current are given in Table III, and the averaged least squares costs and optimization times for each parameter set are given in Table IV.

### C. Whole-Cell AP Model

To generate predictions about the effect of the theoretical modifiers on APD, we used the most recent canine ventricular AP model that is available, the HRd model of the canine epicardial AP [30]. This model includes several important currents and processes that are absent from earlier canine models, including

TABLE IV  
 OPTIMIZATION INFORMATION

	Average least squares cost	Computation time (sec)
Modifier <sub>I</sub>	1.042e-5	1281
Modifier <sub>C3</sub>	1.138e-5	1433
Modifier <sub>O</sub>	5.605e-5	7756

Average least squares costs and computation times for optimizations of HH<sub>Mod</sub> model modifier-effect parameters

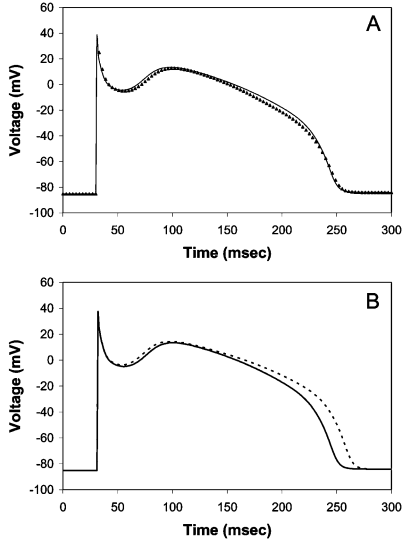


Fig. 4. (A) Simulated APs at 1000 ms generated using original HRd model (triangles) and Markov<sub>MB</sub> substituted  $I_{K,r}$  HRd model (solid line). (B) Simulated epicardial (solid line) and midmyocardial (dotted line) APs at 1000 ms generated using the control HH<sub>Mod</sub>  $I_{K,r}$  model in the HRd AP model.

a formulation of the late sodium current which has been shown to play an important role in heterogeneity of cellular electrical properties [32]. The model is as published in [32] except for the following modifications:

- $[Na^+]_i$ ,  $[K^+]_i$ , and  $[Cl^-]_i$  were fixed at their steady-state values so as to reach steady state more quickly;
- the original Hund–Rudy  $I_{K,r}$  formulation was removed and replaced with either the Markov model of  $I_{K,r}$  described in [32, Sec. 5.1] or the HH model of  $I_{K,r}$  described in [32, Sec. 5.2];
- the model was stimulated with square pulses with duration 1 ms and amplitude 80 mV.

The APs generated by the modified HRd AP models were very similar to those from the original HRd model [see Fig. 4(a)].

The HRd model was modified to reproduce midmyocardial (M) ventricular cells [see Fig. 4(b)] in the following manner:

- $GK_{SM} = 0.5 * GK_{S_{Epi}}$  as reported in Liu [40];
- $GNaL_M = 1.47 * GNaL_{Epi}$  as reported in [32].

It has been reported that there is a less than 10% difference between the sodium–calcium exchange current  $I_{NaCa}$  in M cells and epicardial cells [41]. Therefore, the M cell model used the original  $I_{NaCa}$  current model. We note that the results presented in this paper were duplicated using the ten Tusscher human AP model [33] (data not shown) and were found to be independent of the choice of AP model.

The existing  $I_{K,r}$  component of HRd was replaced with either the Markov<sub>MB</sub> $I_{K,r}$  model described in Section II-A, the Markov<sub>GKr</sub> $I_{K,r}$  model described in Section II-B, or the HH<sub>Mod</sub> $I_{K,r}$  model described in Section II-C, and steady-state APD<sub>90</sub> was measured at various pacing cycle lengths. In the absence of any modifier effects (concentration = 0), all of the substituted  $I_{K,r}$  HRd models produce APs similar to the original HRd. Each of the substituted  $I_{K,r}$  HRd models was also modified to qualitatively reproduce the behavior of midmyocardial myocytes.

#### D. Simulation Details

All simulations and optimizations were run on a Dell Inspiron 9100 computer using custom written C++ computer code. Each ionic model as previously described (either single channel or whole-cell) is represented by a set of differential equations of the form  $dx/dt = f(x, t, p)$ , where  $x$  is a vector describing the current state of the system,  $t$  is time, and  $p$  is a vector of parameters. For the models described, the corresponding differential equations are usually quite stiff in the sense that they have widely separated time scales: some variables change rapidly under small perturbations while others change slowly. To improve the accuracy of our simulations, we used the CVODES package from Lawrence Livermore National Laboratories [34] with the backwards differentiation formula, which is designed for stiff systems. We also used automatic differentiation to calculate the Jacobian derivative of the function  $f$  for use with the dense Newton-based solver that is included as part of CVODES.

For the optimization of models to data, we used the Levenberg–Marquardt local optimizer [31]. The cost for a particular simulation is based on a sum of squares calculation. At each time point for which there is experimental data, the difference between the simulation value and the experimental value is squared. These squares are then summed over all the data points, and the sum represents the cost for that simulation. The optimization problem consists of finding parameters to minimize the cost.

### III. RESULTS

#### A. APD Concentration-Response Predictions

To evaluate the simplifications involved in the Markov<sub>GKr</sub> and HH<sub>Mod</sub> models relative to the Markov<sub>MB</sub> model, we examined predictions of APD concentration-response based on  $I_{K,r}$  ion current data for theoretical modifiers binding the  $C_3$ , O, and I states of the Markov<sub>MB</sub> model. To assess the ability of the models to accurately capture rate-dependent effects, three cycle lengths were studied (CL = 1000, 500, and 300 ms).

As Fig. 5 shows, all three methods produced quantitatively equivalent APD concentration-response predictions for Modifier<sub>I</sub> and Modifier<sub>C3</sub> at a pacing interval of 1000 ms. This result is consistent with those at pacing intervals of 500 and 300 ms (data not shown).

As Fig. 6 shows, the APD concentration-response predictions for Modifier<sub>O</sub> at pacing intervals of 1000 and 300 ms generated by the Markov<sub>GKr</sub> method captured the qualitative trend in the Markov<sub>MB</sub> predictions, but were not quantitatively equivalent, whereas the HH<sub>Mod</sub> predictions were quantitatively equivalent

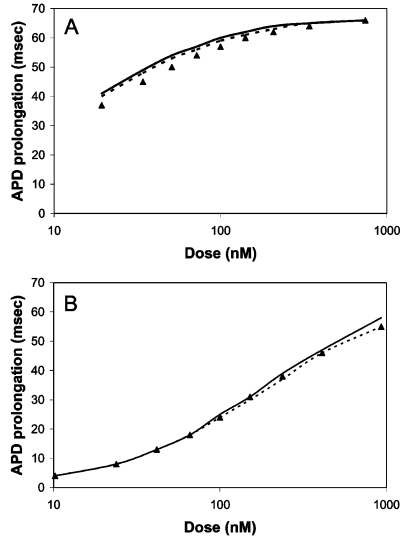


Fig. 5. APD prolongation concentration-response predictions generated by  $\text{Markov}_{\text{MB}}$  (triangles),  $\text{Markov}_{\text{GKr}}$  (dotted lines), and  $\text{HH}_{\text{Mod}}$  (solid lines), paced at  $\text{CL} = 1000$  ms. (A)  $\text{Modifier}_{\text{C3}}$ . (B)  $\text{Modifier}_1$ .

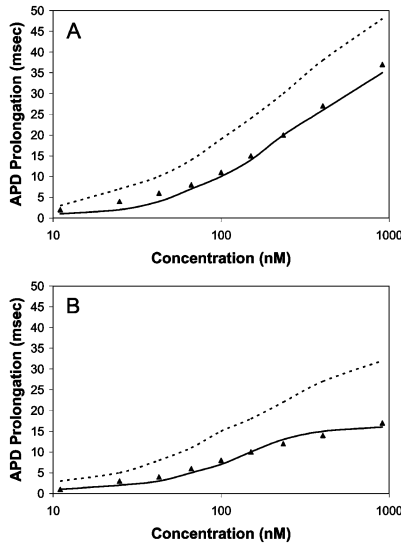


Fig. 6. APD prolongation concentration-response predictions for  $\text{Modifier}_O$  generated by  $\text{Markov}_{\text{MB}}$  (triangles),  $\text{Markov}_{\text{GKr}}$  (dotted lines), and  $\text{HH}_{\text{Mod}}$ . (A)  $\text{CL} = 1000$  ms. (B)  $\text{CL} = 300$  ms.

to the  $\text{Markov}_{\text{MB}}$  model for  $\text{Modifier}_O$ . These results are consistent with those seen at a pacing interval of 500 ms (data not shown). The agreement between  $\text{HH}_{\text{Mod}}$  and  $\text{Markov}_{\text{MB}}$  predictions across pacing cycle length indicate that the  $\text{HH}_{\text{Mod}}$  model was able to reproduce the rate-dependence of  $\text{Modifier}_O$  seen in  $\text{Markov}_{\text{MB}}$ .

#### 1) $I_{K,r}$ Morphology Concentration-Response Predictions:

To explore the failure of  $\text{Markov}_{\text{GKr}}$  to quantitatively reproduce the  $\text{Markov}_{\text{MB}}$  APD concentration-response predictions for  $\text{Modifier}_O$ , we examined the concentration-dependent changes in  $I_{K,r}$  morphology for  $\text{Modifier}_O$  in each of the three models.

As Fig. 7(a) shows, the morphology of the  $\text{Markov}_{\text{MB}}$   $I_{K,r}$  current changes as a function of  $\text{Modifier}_O$  concentration in a

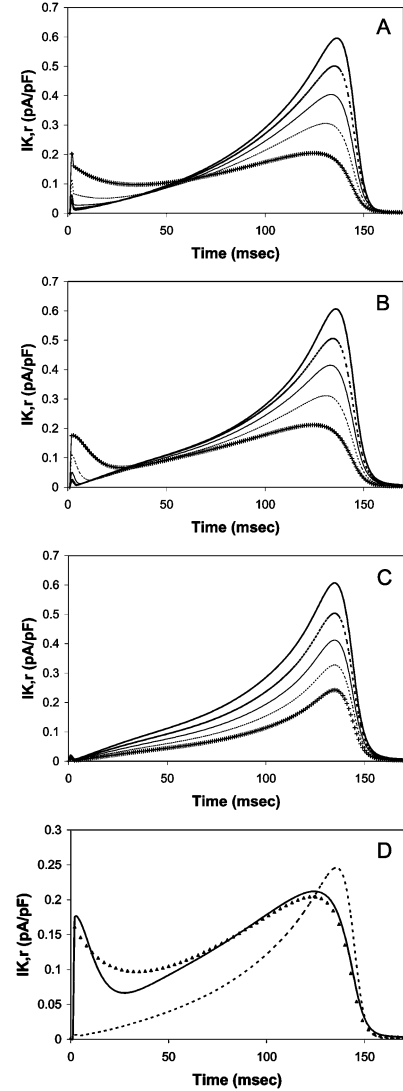


Fig. 7.  $I_{K,r}$  in response to AP clamp stimulation paced at  $\text{CL} = 300$  ms, with  $\text{Modifier}_O = 0$  nM (thick solid lines), 25 nM (thick dotted lines), 67 nM (thin solid lines), 150 nM (thin dotted lines), 403 nM (pluses). (A)  $\text{Markov}_{\text{MB}}$ . (B)  $\text{HH}_{\text{Mod}}$ . (C)  $\text{Markov}_{\text{GKr}}$ . (D) Comparison of  $\text{Markov}_{\text{MB}}$  (triangles),  $\text{Markov}_{\text{GKr}}$  (dotted lines), and  $\text{HH}_{\text{Mod}}$  (solid lines) at  $\text{Modifier}_O = 234$  nM.

nontrivial manner. As concentration increases,  $I_{K,r}$  during repolarization decreases more quickly than  $I_{K,r}$  during the AP plateau. Additionally,  $I_{K,r}$  during the upstroke and notch increases with concentration at shorter cycle lengths. The  $\text{HH}_{\text{Mod}}$  model of the effect of the modifier displays these concentration-dependent behaviors in  $I_{K,r}$  morphology [see Fig. 7(b)]. In contrast, the  $\text{Markov}_{\text{GKr}}$  model cannot capture morphological changes in  $I_{K,r}$  [see Fig. 7(c)] because the  $\text{Markov}_{\text{GKr}}$  model is limited to scaling the amplitude of the  $I_{K,r}$  current. A comparison of the  $I_{K,r}$  traces of the three models at a high concentration of  $\text{Modifier}_O$  [see Fig. 7(d)] clearly demonstrates these morphological differences.

The changes in  $I_{K,r}$  morphology caused by a modifier that binds the open state of the channel have a significant effect on APD (see Fig. 6). This result is of particular interest given that several modifiers (e.g., MK-499 [35], E4031 [35], almokalant [36], dofetilide [37], [38], and ibutilide [37]), are known to bind the open state of the  $I_{K,r}$  channel.

### B. Insights Into Functional Differences Between Modifiers Binding Different Conformational States of $I_{K,r}$

Examination of the simulation results and of the parameters in the  $\text{HH}_{\text{Mod}}$  model allows one to connect the physical interaction of a modifier with the HERG channel to its functional effect on the  $I_{K,r}$  current, providing insight into how the results obtained in the HH model reflect the molecular mechanisms in the  $\text{Markov}_{\text{MB}}$  model. As shown in Table III, reproducing the concentration-response behavior of  $\text{Modifier}_O$  required concentration-dependent changes in  $I_{K,r}$  channel kinetics ( $Q_0 \neq Q_{\text{Inf}}$  for all  $\text{HH}_{\text{Mod}}$  quantities) as well as concentration-dependent reduction of the  $I_{K,r}$  amplitude. The binding of  $\text{Modifier}_O$  resulted in an increase in the activation and inactivation time constants, and positive shifts in the steady-state crossover voltages of both activation and inactivation gates. Conversely, reducing  $I_{K,r}$  amplitude without affecting channel kinetics was sufficient to reproduce the concentration-response behaviors of  $\text{Modifier}_{C_3}$  and  $\text{Modifier}_I$ . The difference in  $GK_r D_{1/2,Q}$  values between  $\text{Modifier}_{C_3}$  and  $\text{Modifier}_I$  indicates that although both modifiers had a similar qualitative effect on  $I_{K,r}$ , and both had the same  $\text{IC}_{50}$  of 100 nM in response to stimulation with a voltage step protocol, the two modifiers had significantly different effective  $\text{IC}_{50}$  values in the AP model. This discrepancy is due to differences in state occupancy dynamics during stimulation with a voltage step protocol versus unclamped AP pacing, as described in the following.

Examination of  $\text{Markov}_{\text{MB}}$  state occupancy probability densities can help elucidate the mechanisms of these functional differences in the effect of the modifier. At rest, the probability density on state  $C_1$  is larger than that of any other state (probability density is localized on  $C_1$ ). When membrane voltage is increased, either during AP upstroke or voltage step from  $-80$  to  $10$  mV, the probability density shifts from localization on  $C_1$  to I, transitioning mainly via  $C_3$  to I inactivation, producing only slight O occupancy and, therefore, little  $I_{K,r}$  current. When membrane voltage is then decreased, either during repolarization or voltage step to  $-50$  mV, probability density shifts from I back to  $C_1$ , via both the I to O transition and the I to  $C_3$  transition, producing significant transient O state occupancy and  $I_{K,r}$  current.

In the presence of  $\text{Modifier}_{C_3}$ , modifier binding occurs when probability density is localized on state  $C_3$ , largely during the inactivation transition from  $C_1$  to I via  $C_3$  [see Fig. 8(a)]. This binding reduces the probability density of state I during inactivation, and, therefore, decreases transient density flow through state O during repolarization, thereby decreasing  $I_{K,r}$  current. However, while the membrane voltage is held at  $10$  mV in the voltage step protocol, probability density gradually transitions from the  $C_3$ -bound state to state I [see Fig. 8(b)], thereby reducing the effect of  $\text{Modifier}_{C_3}$  on  $I_{K,r}$ . This causes long voltage step protocols to underestimate the effect  $\text{Modifier}_{C_3}$  will have on  $I_{K,r}$  during APs. Conversely, since probability density is localized on state I immediately prior to the voltage step from  $10$  to  $-50$  mV and the subsequent occurrence of the  $I_{K,r}$  transient, the effect of  $\text{Modifier}_I$  on  $I_{K,r}$  during APs is accurately captured by such voltage step protocols.

In the presence of  $\text{Modifier}_O$ , some probability density is localized on the  $O_{\text{Bound}}$  state throughout the action potential and

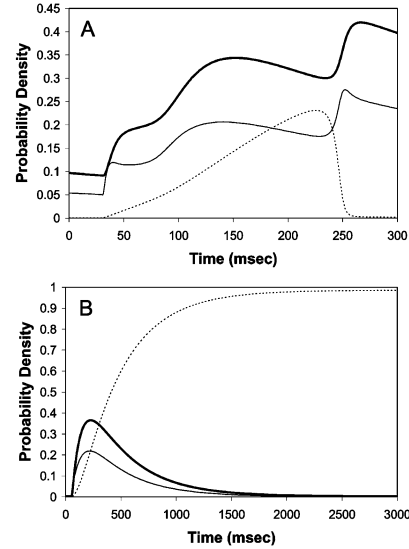


Fig. 8.  $\text{Markov}_{\text{MB}} I_{K,r}$  state occupancy probability density of states  $C_3$  (thin solid line),  $C_{3,\text{Bound}}$  (thick solid line), and I (dotted line), with  $\text{Modifier}_{C_3} = 5$  nM. (A) During AP clamp at  $\text{CL} = 1000$  ms. (B) During voltage step from  $-80$  to  $10$  mV.

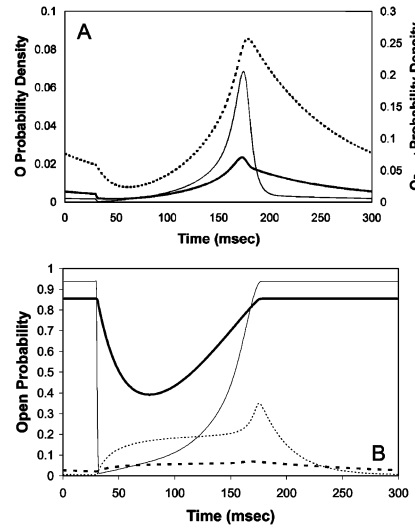


Fig. 9. (A)  $\text{Markov}_{\text{MB}} I_{K,r}$  in response to AP clamp  $\text{CL} = 300$  ms. State occupancy probability densities of state O (control, thin solid line;  $\text{Modifier}_O = 200$  nM, thick solid line) and  $O_{\text{Bound}}$  ( $\text{Modifier}_O = 200$  nM, dotted line). (B)  $\text{HH}_{\text{Mod}} I_{K,r}$  in response to AP clamp  $\text{CL} = 300$  ms. Open probabilities for activation gate X (control, thin dotted line;  $\text{Modifier}_O = 1000$  nM, thick dotted line) and inactivation gate Y (control, thin solid line;  $\text{Modifier}_O = 1000$  nM, thick solid line).

during the rest interval, particularly at high concentrations and rapid pacing rates. During the AP upstroke and plateau, a fraction of this probability density transitions from  $O_{\text{Bound}}$  to I via O, resulting in increased early  $I_{K,r}$ . During repolarization, however, the significant fraction of channels in the  $O_{\text{Bound}}$  state reduces the probability density localized on O, resulting in less late  $I_{K,r}$  [see Fig. 9(a)].

Reproduction of this biphasic response of  $I_{K,r}$  to  $\text{Modifier}_O$  requires a modification of the kinetics of  $I_{K,r}$  in addition to the maximal conductance  $GK_r$ . In the HH model of  $I_{K,r}$ , increasing  $\tau_Y$  and  $R_Y$  results in a greater inactivation gate open

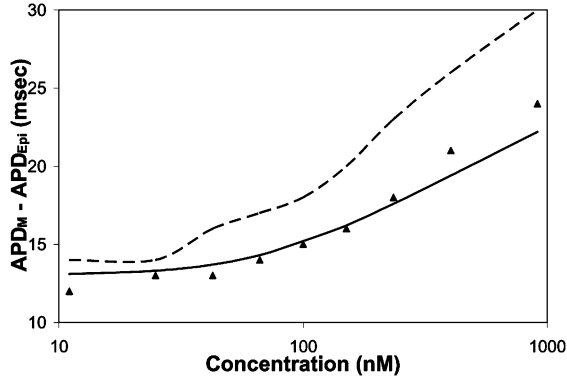


Fig. 10.  $(APD_M - APD_{Epi})$  concentration-response for  $Modifier_O$  at a cycle length of 1000 ms generated by HRd cell model using  $Markov_{MB}$  (triangles),  $Markov_{GKr}$  (dashed line), and  $HH_{Mod}$  (solid line).

probability during upstroke and plateau, and lower open probability during repolarization and rest [see Fig. 9(b), solid lines]. Increasing  $\tau_X$  and  $R_X$  causes an accumulation of activation gate open probability, particularly at high concentrations and fast pacing rates, resulting in an increase in  $I_{K,r}$  during the upstroke and early plateau. The same changes in activation kinetics result in a decrease in open probability, and, therefore, less current, during repolarization [see Fig. 9(b), dotted lines]. These effects, combined with a decrease in  $GKr$ , result in the biphasic  $I_{K,r}$   $Modifier_O$  concentration-response exhibited by  $Markov_{BD}$ .

### C. Intrinsic Electrical Heterogeneity Concentration-Response Predictions

To examine predictions about the effect of the modifier on intrinsic electrical heterogeneity, the HRd AP model, originally designed to describe epicardial (EPI) myocytes, was modified to qualitatively reproduce the behavior of midmyocardial myocytes (M) [26, App. A, Sec. A.3]. The APD concentration-response predictions for  $Modifier_O$  generated by  $Markov_{MB}$ ,  $Markov_{GKr}$  and  $HH_{Mod}$  in these two AP models were then studied. Because preferential prolongation of M cell APD is thought to be arrhythmogenic, we investigated each method's prediction of concentration-dependent changes in the difference between M cell APD ( $APD_M$ ) and EPI cell APD ( $APD_{Epi}$ ).

The  $HH_{Mod}$  model reproduced heterogeneity concentration-response predictions for  $Modifier_O$  generated by the  $Markov_{MB}$  model in a quantitative manner, whereas  $Markov_{GKr}$  did so only qualitatively (see Fig. 10). Simulations at cycle lengths of 500 and 300 ms produced similar results (data not shown).

The simulations also suggest a mechanism for preferential prolongation of M cell APD. In the absence of any modifier, the AP plateau voltage is higher in M cells than in epicardial cells, due to less  $I_{K,s}$  outward current and more  $I_{Na,L}$  inward current. The higher voltage causes an approximately 10% larger driving force ( $V - E_k$ ) at the time of peak  $I_{K,r}$ , and results in an approximately 10% larger peak  $I_{K,r}$  current in M cells than in epicardial cells. Therefore, decreasing  $I_{K,r}$  in M cells has a more significant prolonging effect on APD than in EPI cells.

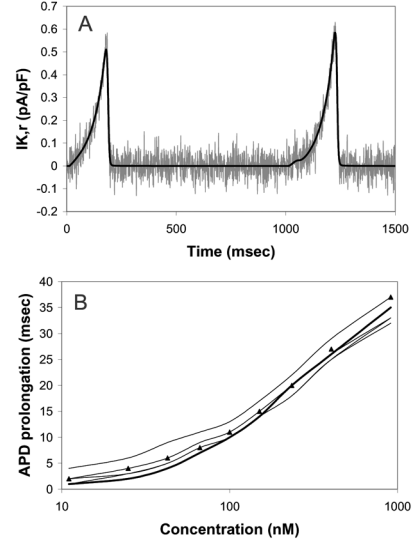


Fig. 11. (A) Untransformed control  $Markov_{MB} I_{K,r}$  trace (black line) and the same trace with one replicate of Gaussian noise added. (B)  $Modifier_O$  APD concentration-response predictions at  $CL = 1000$  ms generated by  $Markov_{MB}$  (triangles),  $HH_{Mod}$  without noise (thick line), and four replicates of  $HH_{Mod}$  with added noise (thin lines).

### D. APD Concentration-Response Predictions in the Presence of Gaussian Noise

To evaluate the effectiveness of the  $HH_{Mod}$  model and the optimization strategy described in Section II-D for reproducing experimental data, Gaussian noise was added to the synthetic data for  $Modifier_O$ . The mean of the noise was set to 0 and the standard deviation was estimated to be to 0.046 pA/pF from experimental  $I_{K,r}$  recordings [29]. Four sets of APD concentration-response predictions for  $Modifier_O$  were generated by fitting to four replicates of  $I_{K,r}$  concentration-response data with random noise. As Fig. 11 shows, the addition of noise did not significantly effect the  $HH_{Mod}$  APD concentration-response predictions.

## IV. DISCUSSION

In this study, we used mathematical models to investigate strategies for using ion current data to predict the effect of channel-binding chemical species on cellular properties such as APD and intrinsic electrical heterogeneity. Our study focused on the delayed rectifier  $K^+$  current  $I_{K,r}$  due to the link between  $I_{K,r}$  block, prolonged APD, amplified intrinsic electrical heterogeneity, and susceptibility to arrhythmias [26], but the methods developed here should be generally applicable to other electrophysiological studies. We compared three methods for quantifying modifier-ion current interactions and generating cellular APD concentration-response predictions that appear to offer the typical tradeoffs between computational efficiency and accuracy of prediction. The results of our simulations suggest a mathematical modeling strategy for characterizing the effect of modifier-ion current interactions on cellular electrophysiological properties that can quantitatively reproduce behaviors from a more computationally demanding approach.

The most complex approach we studied was to model the modifier-ion current interaction through simulation of the physical interaction of the modifier with the channel protein using a Markov model with mass action binding. Such a model can capture a range of dynamic behaviors, and can provide physiological insight into the modifier's mechanism of action. However, if the binding properties of a modifier are unknown, then estimating parameters for the transition rates between all possible bound states is necessary. This method would require the estimation of a large number of parameters simultaneously, which is very computationally expensive. Therefore, a simplified and more computationally efficient method is desirable.

The simplest approach for modeling modifier-ion current interactions that we studied was to scale conductance as a function of modifier concentration. While using this approach in a Markov model qualitatively reproduced the APD concentration-response predictions generated by a Markov model with explicit modifier binding for three theoretical modifiers, scaling the conductance did not quantitatively reproduce the predictions for the open channel binding modifier. Additionally, scaling conductance generated predictions about the effect of the modifier on heterogeneity that were qualitatively, but not quantitatively, consistent with those made by the Markov<sub>MB</sub> model. Therefore, we conclude that for applications that do not require quantitative accuracy, scaling channel conductance is as effective as mass action binding for modeling modifier-ion current interactions. The main advantage of the conductance scaling modeling strategy over others is its simplicity: only four parameters need to be estimated. However, for applications where both computational efficiency and quantitative accuracy are necessary, neither of the previous approaches are adequate.

We have shown that an HH model of  $I_{K,r}$  in which important kinetic parameters are defined as concentration-dependent can quantitatively reproduce the cellular APD concentration-response predictions for several theoretical modifiers generated by a Markov model of  $I_{K,r}$  with mass action binding. By fitting the ion current time series generated in response to an AP clamp at three cycle lengths, the HH<sub>Mod</sub> model was able to reproduce the Markov<sub>MB</sub> concentration-response predictions of  $I_{K,r}$  morphology, APD, and heterogeneity. The HH<sub>Mod</sub> method presented here has computational advantages over Markov models with mass action binding. The HH<sub>Mod</sub> method requires no prior knowledge about the modifier's mechanism of action and binding kinetics. Clearly, this is of great importance when studying novel modifiers. The HH<sub>Mod</sub> method requires the estimation of 21 parameters, which is a more tractable optimization problem than that offered by the Markov<sub>MB</sub> model, particularly when approached in the three-stage manner described in Section II-C.

Such a model of modifier effect on  $I_{K,r}$  could aid researchers in predicting the effect of novel ion current modifiers on cellular and tissue properties. Experimental concentration-response data describing the effect of a novel modifier on  $I_{K,r}$  could be collected, and then the HH modifier-effect model optimized to reproduce the experimental data, as described in Section II-C. This optimized model could then be incorporated into a whole cell AP model, as described in Section II-D, and used to generate predictions about the effect of the modifier on cellular prop-

erties such as action potential duration. Furthermore, the new AP model could then be integrated into a multicell, tissue level model to generate predictions about the effect of the modifier on tissue level properties, such as wave propagation and arrhythmogenesis.

These results suggest promising directions for future experimental work. A logical extension of this study would involve experimental validation of the approach presented here. Experimental data for modifiers binding  $I_{K,r}$  could be fit using the HH<sub>Mod</sub> method, and the model predictions for APD concentration-response checked against experimental results, allowing assessment of the reliability of this method of modeling modifier effect. In addition, the simulation results suggest that voltage step protocols are not ideal for measuring the effect of the modifier on  $I_{K,r}$  during APs, and that development of a more predictive command protocol would be desirable. These efforts will likely benefit from an approach that uses computational methods similar to those presented in this study to help guide experimental design and interpret results.

Although the method presented here reproduced the APD concentration-response data generated using a Markov model with mass action binding, there were several limitations to our study. First, this study only examined modeling of modifier interaction with  $I_{K,r}$  and did not address the development of the control model of the current. However, preliminary tests indicate that the results do not depend sensitively on the control model parameters; several different low cost control HH parameter sets produced very similar results. Second, several simplifying assumptions were used to model modifier binding in the Markov model, such as ignoring explicit voltage-dependence of binding and the spatial distribution of modifier molecules. In addition, it is known that drugs such as cisapride bind more than one state of the HERG channel[39], and this study did not thoroughly explore modifiers that bind multiple states of the channel. However, the HH<sub>Mod</sub> model was able to quantitatively replicate Markov<sub>MB</sub> APD concentration-response predictions for several theoretical compounds that bind more than one conformational state (data not shown), including nonmonotonic concentration-dependent changes in peak  $I_{K,r}$  and APD. In addition, this method could be used in conjunction with a Markov model to develop a thorough understanding of a modifier's mechanism of action and the connection between its binding properties and their functional consequences.

In conclusion, we have proposed an HH-based modeling method that is as predictive as a more complex Markov formulation and reveals the functional effect of modifier-ion current interactions, but that requires no prior knowledge of binding dynamics and fewer computational resources. This method could allow researchers to more easily generate predictions about the effect of novel ion current modifiers on cellular and tissue properties. Such a computational approach could be a powerful tool to help researchers connect the molecular effects of signaling pathways and channel blockers to changes in cellular and tissue behaviors.

#### ACKNOWLEDGMENT

The authors would like to thank Dr. Robert F. Gilmour, Jr. for insightful comments and suggestions, as well as our colleagues

at Gene Network Sciences for their invaluable contributions, in particular to M. Wilks for assistance in completing simulations and to Robert Miller and Basudev Chaudhuri for help with Visual Cell software.

## REFERENCES

- [1] A. L. Hodgkin and A. F. Huxley, "A quantitative description of membrane current and its application to conduction and excitation in nerve," *J. Phys.*, vol. 117, pp. 500–544, 1952.
- [2] B. Hille, *Ionic Channels of Excitable Membranes*. Sunderland, MA: Sinauer Associates, Inc., 1992.
- [3] Y. Kurata, I. Hisatome, S. Imanishi, and T. Shibamoto, "Roles of L-type  $\text{Ca}^{2+}$  and delayed-rectifier  $\text{K}^+$  currents in sinoatrial node pacemaking: Insights from stability and bifurcation analyses of a mathematical model," *Amer. J. Phys. Heart Circ. Phys.*, vol. 285, pp. 2804–2819, 2003.
- [4] G. B. Ermentrout and C. C. Chow, "Modeling neural oscillations," *Phys. Behavior*, vol. 77, pp. 629–633, 2002.
- [5] J. Jo, H. Kang, M. Y. Choi, and D. S. Koh, "How noise and coupling induce bursting action potentials in pancreatic  $\beta$ -cells," *Biophys. J.*, vol. 89, pp. 1534–1542, 2005.
- [6] C. H. Luo and Y. Rudy, "A model of the ventricular cardiac action potential. Depolarization, repolarization, and their interaction," *Circ. Res.*, vol. 68, pp. 1501–26, Jun. 1991.
- [7] D. DiFrancesco and D. Noble, "A model of cardiac electrical activity incorporating ionic pumps and concentration changes," *Philos. Trans. R. Soc. London B Biol. Sci.*, vol. 307, pp. 353–98, Jan. 1985.
- [8] J. P. Keener and J. Sneyd, *Mathematical Physiology*. New York: Springer, 1998.
- [9] R. Mazhari, J. L. Greenstein, R. L. Winslow, E. Marban, and H. B. Nuss, "Molecular interactions between two long-QT syndrome gene products, HERG and KCNE2, rationalized by in vitro and in silico analysis," *Circ. Res.*, vol. 89, pp. 33–8, Jul. 2001.
- [10] E. X. Albuquerque, J. W. Daly, and J. E. Warnick, "Macromolecular sites for specific neurotoxins and drugs on chemosensitive synapses and electrical excitation in biological membranes," *Ion Channels*, vol. 1, pp. 95–162, 1988.
- [11] R. Malek, K. K. Borowicz, Z. Kimber-Trojnar, G. Sobieszek, B. Piskorska, and S. J. Czuczwar, "Remacemide—A novel potential antiepileptic drug," *Pol. J. Pharmacol.*, vol. 55, pp. 691–698, 2003.
- [12] T. J. Kamp and J. W. Hell, "Regulation of cardiac L-type calcium channels by protein kinase A and protein kinase C," *Circ. Res.*, vol. 87, pp. 1095–102, Dec. 2000.
- [13] H. L. Tan, S. Kupersmidt, R. Zhang, S. Stepanovic, D. M. Roden, A. A. M. Wilde, M. E. Anderson, and J. R. Balsler, "A calcium sensor in the sodium channel modulates cardiac excitability," *Nature*, vol. 415, pp. 442–447, Jan. 2002.
- [14] J. Cui, Y. Melman, E. Palma, G. I. Fishman, and T. V. McDonald, "Cyclic AMP regulates the HERG  $\text{K}^+$  channel by dual pathways," *Curr. Biol.*, vol. 10, pp. 671–4, Jun. 2000.
- [15] W. Haverkamp, G. Breithardt, A. J. Camm, M. J. Janse, M. R. Rosen, C. Antzelevitch, D. Escande, M. Franz, M. Malik, A. Moss, and R. Shah, "The potential for QT prolongation and pro-arrhythmia by non-anti-arrhythmic drugs: Clinical and regulatory implications. Report on a policy conference of the European society of cardiology," *Cardiovasc. Res.*, vol. 47, pp. 219–33, Aug. 2000.
- [16] J. S. Mitcheson, J. Chen, M. Lin, C. Culberson, and M. C. Sanguinetti, "A structural basis for drug-induced long QT syndrome," in *Proc. Nat. Acad. Sci. USA*, 2000, pp. 12329–33.
- [17] B. Fermini and A. A. Fossa, "The impact of drug-induced QT interval prolongation on drug discovery and development," *Nat. Rev. Drug Discovery*, vol. 2, pp. 439–47, Jun. 2003.
- [18] C. Antzelevitch, L. Belardinelli, A. C. Zygmunt, A. Burashnikov, J. M. D. Diego, J. M. Fish, J. M. Cordeiro, and G. Thomas, "Electrophysiological effects of ranolazine, a novel antianginal agent with antiarrhythmic properties," *Circulation*, vol. 110, pp. 904–10, Aug. 2004.
- [19] D. Bottino, R. C. Penland, A. Stamps, M. Traebert, B. Dumotier, A. Georgieva, G. Helmlinger, and G. S. Lett, "Preclinical cardiac safety assessment of pharmaceutical compounds using an integrated systems-based computer model of the heart," *Progress Biophys. Molecular Bio.*, vol. 90, pp. 414–443, Jul. 2005.
- [20] J. M. Ridley, J. T. Milnes, Y. H. Zhang, H. J. Witchel, and J. C. Hancox, "Inhibition of HERG  $\text{K}^+$  current and prolongation of the guinea-pig ventricular action potential by 4-aminopyridine," *J. Phys.*, vol. 549, pp. 667–672, Jun. 2003.
- [21] A. Zaza, M. Micheletti, A. Brioschi, and M. Rocchetti, "Ionic currents during sustained pacemaker activity in rabbit sino-atrial myocytes," *J. Phys.*, vol. 505, pp. 677–88, Dec. 1997.
- [22] G. J. Amos, I. Jacobson, G. Duker, and L. Carlsson, "Block of HERG-carried  $\text{K}^+$  currents by the new repolarization delaying agent H 345/52," *J. Cardiovascular Electrophys.*, vol. 14, pp. 651–658, Jun. 2003.
- [23] T. Doerr, R. Denger, and W. Trautwein, "Calcium currents in single SA nodal cells of the rabbit heart studied with action potential clamp," *Pflugers Archiv: Eur. J. Phys.*, vol. 413, pp. 599–603, Apr. 1989.
- [24] G. E. Kirsch, E. S. Trepakova, J. C. Brimacombe, S. S. Sidach, H. D. Erickson, M. C. Kochan, L. M. Shyja, A. E. Lacerda, and A. M. Brown, "Variability in the measurement of HERG potassium channel inhibition: Effects of temperature and stimulus pattern," *J. Pharmacology Toxicology Methods*, vol. 50, pp. 93–101, Sep./Oct. 2004.
- [25] L. A. Irvine, M. S. Jafti, and R. L. Winslow, "Cardiac sodium channel Markov model with temperature dependence and recovery from inactivation," *Biophys. J.*, vol. 76, pp. 1868–85, Apr. 1999.
- [26] J. M. D. Diego, L. Belardinelli, and C. Antzelevitch, "Cisapride-induced transmural dispersion of repolarization and torsade de pointes in the canine left ventricular wedge preparation during epicardial stimulation," *Circulation*, vol. 108, pp. 1027–33, Aug. 2003.
- [27] C. F. Starmer, A. Grant, and H. C. Strauss, "Mechanisms of use-dependent block of sodium channels in excitable membranes by local anesthetics," *Biophys. J.*, vol. 46, pp. 15–17, Jul. 1984.
- [28] F. R. Gilliam, C. F. Starmer, and A. O. Grant, "Blockade of rabbit atrial sodium channels by lidocaine. Characterization of continuous and frequency-dependent blocking," *Circ. Res.*, vol. 65, pp. 723–39, Sep. 1989.
- [29] F. Hua and R. F. Gilmour, Jr, "Contribution of  $I_{Kr}$  to rate-dependent action potential dynamics in canine endocardium," *Circ. Res.*, vol. 94, pp. 810–9, Apr. 2004.
- [30] T. J. Hund and Y. Rudy, "Rate dependence and regulation of action potential and calcium transient in a canine cardiac ventricular cell model," *Circulation*, vol. 110, pp. 3168–74, Nov. 2004.
- [31] D. Marquardt, "An algorithm for least-squares estimation of nonlinear parameters," *SIAM J. Appl. Math.*, vol. 11, pp. 431–441, 1963.
- [32] A. C. Zygmunt, G. T. Eddlestone, G. P. Thomas, V. V. Nesterenko, and C. Antzelevitch, "Larger late sodium conductance in M cells contributes to electrical heterogeneity in canine ventricle," *Amer. J. Phys.*, vol. 281, pp. H689–97, Aug. 2001.
- [33] K. H. t. Tusscher, D. Noble, P. J. Noble, and A. V. Panfilov, "A model for human ventricular tissue," *Amer. J. Phys. Heart Circ. Phys.*, vol. 286, pp. H1573–89, Apr. 2004.
- [34] S. D. Cohen and A. C. Hindmarsh, "CVODE user guide," LLNL, UCRL-MA-118618, Oct. 1994 [Online]. Available: <http://robotics.stanford.edu/~scohen/cvuguide.pdf>
- [35] P. S. Spector, M. E. Curran, M. T. Keating, and M. C. Sanguinetti, "Class III antiarrhythmic drugs block HERG, a human cardiac delayed rectifier  $\text{K}^+$  channel. Open-channel block by methanesulfonanilides," *Circ. Res.*, vol. 78, pp. 499–503, Mar. 1996.
- [36] E. Carmeliet, "Use-dependent block and use-dependent unblock of the delayed rectifier  $\text{K}^+$  current by almokalant in rabbit ventricular myocytes," *Circ. Res.*, vol. 73, pp. 857–868, 1993.
- [37] T. Yang, M. S. Wathen, A. Felipe, M. M. Tamkun, D. Snyders, and D. Roden, " $\text{K}^+$  currents and  $\text{K}^+$  channel mRNA in cultured atrial cardiac myocytes (AT-1 cells)," *Circ. Res.*, vol. 75, pp. 870–878, 1994.
- [38] E. Carmeliet, "Voltage- and time-dependent block of the delayed rectifier  $\text{K}^+$  current in cardiac myocytes by dofetilide," *J. Pharmacology Exp. Therapy*, vol. 262, pp. 809–817, 1992.
- [39] B. D. Walker, C. B. Singleton, J. A. Bursill, K. R. Wyse, S. M. Valenzuela, M. R. Qiu, S. N. Breit, and T. J. Campbell, "Inhibition of the human ether-a-go-go-related gene (HERG) potassium channel by cisapride: Affinity for open and inactivated states," *Br. J. Pharmacology*, vol. 128, pp. 444–50, Sep. 1999.
- [40] D. W. Liu and C. Antzelevitch, "Characteristics of the delayed rectifier current ( $I_{Kr}$  and  $I_{Ks}$ ) in canine ventricular epicardial, midmyocardial, and endocardial myocytes. A weaker  $I_{Ks}$  contributes to the longer action potential of the M cell," *Circ. Res.*, vol. 76, pp. 351–65, Mar. 1995.
- [41] A. C. Zygmunt, R. J. Goodrow, and C. Antzelevitch, "INaCa contributes to electrical heterogeneity within the canine ventricle," *Amer. J. Physiol.*, vol. 278, pp. H1671–8, May 2000.